International Journal of Biological Macromolecules 278 (2024) 135282

Contents lists available at ScienceDirect

International Journal of Biological Macromolecules

journal homepage: www.elsevier.com/locate/ijbiomac

Synthesis of bio-polyol-functionalized nanocrystalline celluloses as reactive/reinforcing components in bio-based polyurethane foams by homogeneous environment modification

Selena Silvano [a], Pierluigi Moimare [a], Liudmyla Gryshchuk [b], Einav Barak-Kulbak [c], Federica Recupido [d], Giuseppe Cesare Lama [d,*], Laura Boggioni [a,*], Letizia Verdolotti [d]

[a] Institute of Chemical Sciences and Technologies – "G. Natta", Italian National Research Council, via A. Corti 12, 20133 Milan, Italy
[b] Leibniz-Institut für Verbundwerkstoffe GmbH, Technische Universität, Erwin-Schrödinger, straße 58, 67663 Kaiserlauntern, Germany
[c] Melodea Ltd., 7610001 Rehovot, Israel
[d] Institute of Polymers, Composites and Biomaterials, Italian National Research Council, Piazzale E. Fermi 1, 80055 Portici, Italy

ARTICLE INFO

Keywords:
CNC modification
Homogeneous chemical environment
Bio-based polyols
Bio-based polyurethane foams

ABSTRACT

Nanocrystalline Cellulose (NCC or CNC) is widely used as a filler in polymer composites due to its high specific strength, tensile modulus, aspect ratio, and sustainability.

However, CNC hydrophilicity complicates its dispersion in hydrophobic polymeric matrices giving rise to aggregate structures and thus compromising its reinforcing action. CNC functionalization in a homogeneous environment, through silanization with trichloro(butyl)silane as a coupling agent and subsequent grafting with bio-based polyols, is herein investigated aiming to enhance CNC dispersibility improving the filler-matrix interaction between the hydrophobic PU and hydrophilic CNC. The modified CNCs (*m*_Ci) have been studied by XRD, SEM, and TGA analyses. The TGA results show that the amount of grafted polyol is strongly influenced by both its molar mass and OH number and the maximum amount of grafted polyol reaches up to 0.32 mmol per grams of functionalized CNC, within the explored conditions. The effect of different concentrations (1–3 wt%) of *m*_Ci on the physical, morphological, and mechanical properties of the resulting bio-based composite polyurethane foams is evaluated. Composite PU foams present compressive modulus up to 4.81 MPa and strength up to 255 kPa more than five times higher than those reinforced with unmodified CNC or with modified CNC in heterogeneous chemical environment. The improvement of mechanical properties of the examined PU foams, as a consequence of the incorporation of bio-polyols modified CNCs where polyol's OH groups interact with polyurethane precursors, could further broaden the use of these materials in building applications.

1. Introduction

In the last decades, the development of renewable materials and eco-friendly processes has gained much interest, aiming to minimize the carbon footprint as well as fossil fuel dependence [1]. On this account, the research community has widely carried out the replacement of widespread petroleum-derived materials with more environmentally friendly alternatives. Concerning the plastic sector, particularly the polyurethanes (PUs) and PU foams, whose market was estimated at USD 78 billion in 2023 and is expected to grow further to USD 112.5 billion in 2030 [2], the use of bio-based renewable materials, such as bio-based polyols or isocyanate compounds, plays a significant role in promoting waste reduction and sustainable development [3,4].

PU foams represent a broad class of thermosetting polymers [5–7] obtained from simultaneous polyaddition reactions between polyols' OH groups and di-isocyanates' NCO groups, leading to urethane groups, and blowing reaction [8–10]. This latter can be obtained either through the use of physical low boiling point blowing agents (i.e. hydrocarbons, hydrofluorocarbons, etc) which typically change phase from liquid to gas during the polymerization, increasing volume mixture and thus expanding or, through the addition of chemical blowing agents (i.e., H_2O), able to react with isocyanates, producing in-situ CO_2 [8,10]. The type and the amount of the two precursors as well as the use of suitable additives (catalysts, blowing agents, and flame retardants) tailor specific

* Corresponding authors.
E-mail addresses: giuseppecesare.lama@cnr.it (G.C. Lama), laura.boggioni@cnr.it (L. Boggioni).

https://doi.org/10.1016/j.ijbiomac.2024.135282
Received 29 March 2024; Received in revised form 5 August 2024; Accepted 1 September 2024
Available online 10 September 2024

characteristics. According to their morphologies, PU foams can be classified as flexible (having open cells) and rigid (with closed cells) [11]. Intermediate systems, i.e. semirigid, can also be developed. As a result, PU foams present versatile features that enable them to apply in different sectors from construction or packaging/transportation (i.e., for cultural heritage applications) to bedding/cushioning, automotive, and aerospace sectors [4,6,9,11]. Typically, PU foam precursors are petrol-based materials, therefore, to fulfil the principle of circular economy, precursors coming from vegetable or biomass sources or non-isocyanate compounds have been employed instead of conventional materials [12]. Moreover, the introduction of micro- or nano-reinforcing fillers coming from natural or biomass or waste sources such as organic (lignin-cellulosic, chitin, food wastes such as wall nutshell [4] or eggshells and hemp or proteins) and inorganic-based ones (such as clays, diatomite, zeolites, silica, fly ashes and so forth) within PU matrices allows to improve the functional characteristics of the foams such as compressive stress, flame retardancy, thermal conductivity, sound [13,14] and water adsorption [15].

Nanocrystalline Cellulose (NCC or CNC) is broadly recognized as a reinforcing material for polymer composites due to specific features: renewability, high aspect ratio, non-toxicity, biocompatibility, stereoregularity and multichirality. CNC is composed of repeated units of D-glucose linked by glycosidic β(1 → 4) bonds and presents a large number of intramolecular and intermolecular hydrogen bonding interactions between oxygen atoms and hydroxyl groups of hydro-D-glucopyranose units resulting in a polymer containing highly structured crystalline regions, with high tensile strength and modulus [1]. In the specific case of PU foamed materials, CNC has been selected as a filler in rigid or semi-rigid PU foams resulting in improved polymer crosslinking, thus imparting enhanced thermal insulation and mechanical characteristics with respect to the unloaded foams [16,17].

However, the inherent hydrophilicity of CNC often represents a substantial challenge for its application as a reinforcing filler as it complicates its dispersion in hydrophobic polymeric matrices resulting in aggregate structures that compromise the final properties of composite materials [18,19], therefore, the quality of the dispersion and the polymer-filler interaction are crucial factors. Routes based on physical modification, such as the ball-milling of CNC or ultrasonication-based dispersion within PU foam matrices, have been indicated in the literature to improve the CNC dispersion. Stanzione et al. selected the ball milling route to modify CNC obtaining amorphous cellulose (AC), which was found much more dispersed in the PU matrix than unmodified CNC, tuning the PU mechanical properties from rigid-brittle (for unloaded PU and PU-crystalline cellulose foams) to semi-rigid (for the PU-milled cellulose foams) [20]. Recently, Septevani et al. reported a modification of CNC through ultrasonication, revealing that no significant alterations of CNC as well as no improvements of its thermal insulating properties were noted in the resulting composite foams [21].

Surface modification of CNC through chemical routes has been also developed to influence CNC dispersion, interfacial interaction, and the final properties of composite materials. Examples of surface functionalization routes such as polymer grafting, esterification, 2,2,6,6-tetramethylpiperidine-1-oxyl (TEMPO) radical-mediated oxidation, surfactant absorption, carbamation, maleization, silanization have been widely reported in the literature [18,20,22,23]. Silanization is a well-known surface-modification reaction of hydrophilic compounds such as wood [24], starch [25] and cellulosic materials [18,26–28]. Alkyl silane compounds act as a bridge between the hydrophilic and the hydrophobic moieties improving the dispersion of hydrophilic compounds in hydrophobic matrices, resulting in the enhancement of the interfacial adhesion between cellulose and the polymer matrix [29,30]. The type of modification, aiming to improve the dispersion of CNC in the polymer matrix, effectively depends on the type of polymer matrix that CNC must interact with. In the case of PU formulation, the introduction of reactive or compatible groups with polyurethane precursors (polyols or isocyanates) on CNC surface can improve its dispersion in the PU matrix.

A few works focused on using functionalized CNC, where isocyanate groups or polyols were introduced on CNC surface, as a reactive component in PU matrices, however, they mainly refer to thermoplastic or waterborne polyurethane-based composites [26,31,32].

To the best of our knowledge, chemical functionalization pathways preferentially take place in heterogeneous environments in which CNC is dispersed in the reaction medium [23,33]. In fact, the presence of strong hydrogen bond network as well as stereoregularity and crystalline domains makes difficult CNC solubilization in common organic solvents, where, typically, functionalization reactions occur [34]. Chemically modified nanocrystalline celluloses (*m*_CNCs), through the combination of silanization and polyol-grafting, were selected as fillers in PU foams [26]. In this work, a functionalization route in heterogeneous environment has been proposed obtaining *m*_CNCs in which the polyol grafted on the CNC surface was able to react with polyurethane matrix, affecting positively mechanical properties with respect to the unloaded PU foams, and to those reinforced with unmodified CNC, by preserving the crystalline structure.

In this work, the interaction between polyol's OH groups grafted on CNC and isocyanate moiety to enhance the compatibility and interfacial adhesion filler-matrix was exploited. Here, a novel approach to functionalize CNC by silane-polyol grafting in *homogeneous environment* as a method to deeply modify the structure of the CNC and its use as a reinforcing agent in hydrophobic matrices, such as bio-based polyurethane foams, is reported. The dissolution of CNC in an appropriate solvent allowed to break the hydrogen bond within cellulose chains and, in this way, to make its non-surface-hydroxyl groups available for the functionalization allowing a maximization in the amount of grafted polyol.

Silanization was carried out by selecting an eco-friendly and low-cost solvent system: *N*,*N*-dimethylacetamide/lithium chloride (DMAc/LiCl). Subsequent grafting was done by using three bio-based polyols, obtained from different renewable sources. The influence of molar mass and OH number of bio-based polyols on the ability to functionalize the silane-cellulose network was examined and the properties of the so-modified CNCs were analysed by thermal, chemical-physical, and morphological characterizations. The amount of grafted polyol was hence estimated through the well-known Fathi and Rachini equation [35,36].

Successively, modified CNCs were dispersed in bio-based PU foams at three different concentrations (e.g. 1, 2, and 3 wt%). At each different concentration, the effect of functionalization on thermal, morphological, and mechanical properties of the obtained foam was investigated. Finally, a modified Gibson-Ashby model was proposed to connect foam morphological features with its mechanical properties.

2. Experimental

2.1. Materials and chemicals

The bio-based-polyester polyols RV33 (OH_n = 78 mg KOH/g), RV31 (OH_n = 297 mg KOH/g), RV29 (OH_n = 229 mg KOH/g) were supplied by AEP Polymers S.r.l. (Basovizza, Trieste, Italy).

N,*N*-dimethylacetamide (DMAc), triethylamine (TEA), lithium chloride (LiCl), tetrahydrofuran (THF), calcium hydride (CaH_2), and methanol (MeOH) were purchased from Sigma-Aldrich (St. Louis, MO, USA).

Trichloro(butyl)silane (97 %) was acquired from Fisher Scientific (Waltham, MA, USA). Cardolite® NX-9201 (bio-polyester diol, OH_n = 65–80 mg KOH/g) was purchased by Cardolite Corporation (Bristol, PA, USA), Sovermol® 750 (OH_n = 300–330 mg KOH/g) and Sovermol® 815 branched polyester/polyether polyol, OH_n = 200–300 mg KOH/g) were purchased by BASF and used as polyols in PU formulation together with RV33. Glycerol (functionality = 3) was purchased by Sigma-Aldrich (St. Louis, MO, USA) and used as a cross-linking agent. Exolit® OP 560 (co-reactive flame retardant, OH_n = 450 mg KOH/g) was purchased by Clariant (Muttenz, Switzerland). Gelling and blowing catalysts, Dabco®

33-LV and Dabco® NE 300, and silicone based-surfactant TEGOSTAB® B 8747 LF2 were purchased from Evonik (Essen, Germany). Poly(4,4'-Diphenylmethandiisocyanate, p-DMI), Lupranate M20S with 31.5 % NCO content was purchased from BASF (Ludwigshafen am Rhein, Germany). Bi-distilled water was used as an eco-friendly blowing agent.

DMAc and TEA were distilled over CaH_2 before use. Other reagents were used without purification. CNC was supplied by MELODEA Ltd. (Rehovot, Israel) as a 3 wt% aqueous suspension of an average density of 1.3 g•cm^{-3} and viscosity of 2000 mPa•s and indicated in the text as pristine CNC (*p*_C). Particle size distribution was evaluated through Transmittance Electron Microscopy (TEM) resulting in an average width of 6.8 nm (2–20 nm) and length of 170 nm (20–500 nm). The sulphur content of the selected systems was in the range of 10–160 mmol•kg^{-1}. Before use, CNC was freeze-dried at $T = -53$ °C and $P = 0.08$ bar (liophilizer LIO—5P, Cinquepascal S.R.L, Trezzano Sul Naviglio, Italy). The freeze-dried CNC is indicated as unmodified CNC (*u*_C) (see Fig. S1 (a) in Supplementary Material, SM).

2.2. Preparation of polyol-grafted CNCs (*m*_C*i*)

The modification of CNC was performed according to 3 main steps procedure: (1) solubilization of *u*_C to obtain the CNC solution (named as *u*_C_sol), (2) silanization and (3) polyol grafting (Scheme 1). In detail, *u*_C (1.01 g) was suspended at 160 °C for 1 h in DMAc (50 mL) and poured into a two-necked round bottom flask under nitrogen atmosphere. Then, the suspension was cooled down to 100 °C and anhydrous LiCl (3.9 g) was added (Fig. S1 (b), SM) The suspension was kept at 100 °C under vigorous stirring until a homogeneous solution was obtained (Scheme 1, (1)). Afterwards, TEA (1.1 eq) and trichloro(butyl) silane (1.1 eq) were added to *u*_C_sol. The reaction was kept at 70 °C for 2 h under nitrogen atmosphere. After silanization, a further amount of TEA (1.1 eq) and bio-based polyol (1.1 eq) were added (Scheme 1, (2)). The reaction was left at 100 °C overnight under nitrogen atmosphere. The resulting product (Fig. S1 (c)) was isolated through vacuum filtration and the unreacted silane and polyol were removed with tetrahydrofuran and methanol by two consecutive Soxhlet extractions. The wet powder was dried in a vacuum oven (100 mbar) at 80 °C (Scheme 1, (3)).

Three bio-based polyols were employed as grafting agents to synthesize the modified CNCs named as *m*_Ci, where "i" is the number corresponding to the grafted polyol. Chemical characteristics of the polyols employed are summarized in Table 1 and their FT-IR spectra are reported in Section S2, SM.

Table 1
Chemical characteristics of the bio-based polyols used for grafting.

Polyol number (i)	Polyol name	Source	OH_n (mg KOH/g)	M_w (g/mol)	$Đ$[a]
1	RV33	Cardanol and sunflower oil	78	3400	2.4
2	RV31	Cardanol and linseed oil	297	5200	6.2
3	RV29	Cardanol and sunflower oil	229	870	1.5

[a] $Đ$: polydispersity index, $Đ = M_w/M_n$, where M_n is the numerical average molar mass and M_w is the weight average molar mass, see the details of characterization in the SM paragraph S2.

2.3. Preparation of bio-based composite PU foams

Bio-based PU foams were prepared using a one-step method. At first, a solution consisting of a blend of bio-based polyols RV33, Cardolite® NX-9201 Sovermol® 750, Sovermol® 815, and glycerol was prepared. All the additives (catalysts, flame retardant, cell stabilizers, and blowing agent) were added to the polyol blend and the resulting solution (denoted as *Component A*) was mixed for 5 min at 500 rpm. Subsequently, *m*_Ci was added to *Component A* to achieve three different concentrations: 1, 2 and 3 wt%. This concentration range was chosen as comparison with a previous work, where the effect of this CNC concentration range on the compression properties of composite materials was studied [26].

Next, an appropriate amount ([NCO]/[OH] = 1.05) of p-DMI (*Component B*) was added to *Component A* and the reactive mixture was stirred for 20 s at 500 rpm and then transferred in a cylindrical mold, allowing to freely rise at room temperature (composition for 100 g of total foam mass is shown in Table S1, SM).

For sake of brevity, the composite foams were named as PU_ *m*_Ci _y, where "i" is the number corresponding to grafted polyol and "y" is referred to wt% of modified CNC added to PU matrix. Foams with unmodified CNC (named as PU_*u*_C) and unloaded PU foam (PU-Pristine) were used as references (Table 2).

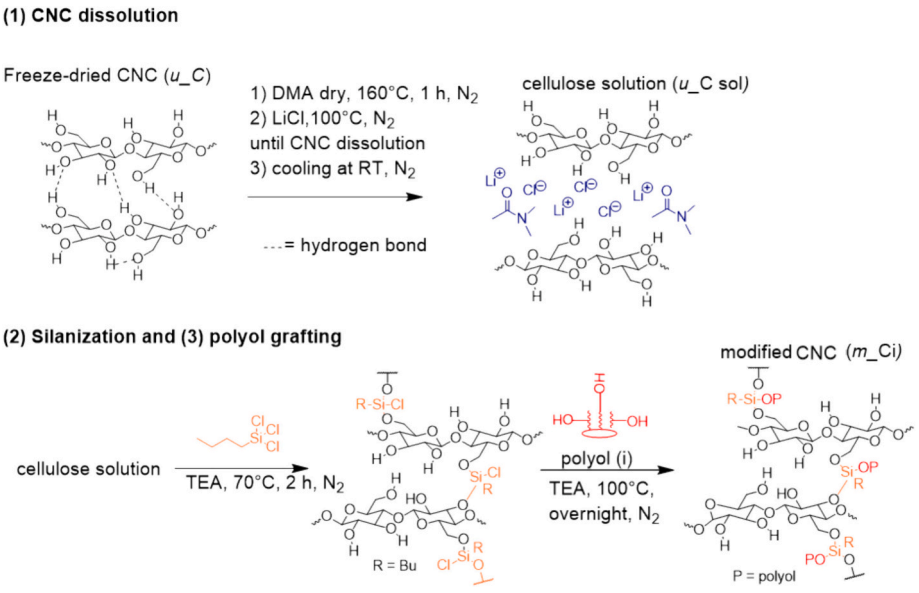

Scheme 1. Sequence of CNC functionalization to obtain modified CNCs (*m*_Ci). 1) Dissolution of CNC in DMAc/LiCl system, resulting in *u*_C_sol product. 2) Silanization and 3) Polyol grafting.

Table 2
Sample name and feed composition of modified CNCs with trichloro(butyl) silane and bio-based polyols.

Modified CNCs	Polyol number (i)	Trichloro(butyl)silane		Polyol	
		eq	mmol	eq	g
*u*_C	–	–	–	–	–
*m*_C1	1	1.1	6.85	1.1	4.93
*m*_C2	2	1.1	6.85	1.1	1.29
*m*_C3	3	1.1	6.85	1.1	1.68

2.4. Characterization methods

2.4.1. Spectroscopic characterization

X-ray diffractometry analysis of CNC before and after functionalization was performed by means of an Anton Paar XRD Dynamic 500 instrument, emitting CuKα radiation scanning (2θ) between 5° and 70°.

*m*_Ci and composite PU foams were characterized by FT-IR (Fourier Transformed Infrared) Spectroscopy (Perkin Elmer Spectrum Two) in Attenuated Total Reflectance (ATR) mode within the range of wavenumber of 400–4000 cm^{-1}, 4 cm^{-1} resolutions and 64 scans. Spectra were normalized between 0 and 100 on transmittance value.

2.4.2. Thermal characterization

Thermogravimetric analysis (TGA) and Derivative Thermogravimetric Analysis (DTGA) were conducted for modified CNCs at 20 °C min^{-1} from 50 °C to 750 °C under nitrogen atmosphere (flow rate of 20 mL min^{-1}) followed by an isothermal step at 750 °C under oxidative atmosphere for 10 min (flow rate of 30 mL min^{-1}). The amount of grafted polyol onto modified CNC (Eq. 1) was assessed by TGA analysis and estimated through Fathi and Rachini's equation [35,36].

$$\text{Grafted polyol}\left(\frac{mmol}{g_{sample}}\right)=\frac{\left[Wt\%m\_Ci_{150^\circ C}-Wt\%m\_Ci_{400^\circ C}-\left(\frac{wt\%_{m\_Ci_{750^\circ C}}}{MM_{SiO2}}*MM_{\text{hydrolized silane}}\right)\right]*1000}{[100*M_w]} \quad (1)$$

$Wt\%_{m\_Ci150^\circ C}$ and $Wt\%_{m\_Ci400^\circ C}$ are the residual masses % of *m*_Ci between 150 °C and 400 °C; $wt\%_{m\_Ci750^\circ C}$ is the residual mass of *m*_Ci at 750 °C in oxidant atmosphere. This latter is attributed to SiO_2 generated from silane oxidation. $MM_{hydrolizated\ silane}$ and M_w are the molar masses of the hydrolysed silane and grafting polyol (g/mol), respectively.

TGA analysis was conducted on PU foams from 30 °C to 800 °C with a heating rate of 10 °C min^{-1} under inert atmosphere (flow rate of 40 mL•min^{-1}).

2.4.3. Morphological characterization

To evaluate *m*_Ci dispersion within *Component A*, optical microscopy images were acquired (model Z16 APO, Leica Microsystems GmbH) at 20 X magnification. Morphological analysis of both CNC and foams was assessed by Scanning Electron microscopy (SEM, FEI Quanta 200) at an acceleration voltage of 20 kV and different magnifications. Samples were sputter-coated with gold/palladium before imaging. For foamed materials, the open-source Image J software was used to analyse the average size, size distribution, and the number of cells per unit of surface (μm^{-2}). For each sample, the above-mentioned parameters were calculated from approximately 100 different cells.

2.4.4. Mechanical characterization

The apparent density of PU foams (ρ, kg•m^{-3}) was determined at 23 °C with 50 % relative humidity (ASTM D1622–03) and estimated as the average value of 10 specimens with size 30 mm × 30 mm × 30 mm (length × width × thickness).

Compressive analysis of PU foams was determined according to DIN EN ISO 844 and carried out through Zwick 1445 Retroline machine (ZwickRoell GmbH and Co. KG). The following parameters were set: initial load 0.5 N, *E*-modulus velocity 10 mm min^{-1}, testing velocity 10 % min^{-1}, maximal deformation 70 %. Compressive strength at 10 % ($\sigma_{10\%}$, MPa), compressive elastic modulus (E_{mod}, MPa) and specific compressive stress (σ/ρ, MPa/kg/m^3) and elastic modulus (E_{mod}/ρ, MPa/kg/m^3) were calculated. These latter ones were obtained by normalizing $\sigma_{10\%}$ and E_{mod} with respect to the apparent density.

3. Modelling

A modified Gibson-Ashby model [14], was used for an in-deep structural characterization of the obtained foams when compression tests were performed, identifying a linear elasticity behaviour. The standard equation is defined as follows (Eq. (2)) [37]:

$$\frac{E}{E_S}=C\varphi^2\left(\frac{\rho}{\rho_S}\right)^2+C'(1-\varphi)\left(\frac{\rho}{\rho_S}\right) \quad (2)$$

Two main factors are considered: E/E_S, the relative modulus, and ρ/ρ_S, the relative density. The first is obtained dividing *E*, the foam compressive modulus (MPa), by E_S, the compressive modulus of the material constituting the cells (set equal to 45 MPa, being semi-rigid PU foams) [37], while the second comes from the ratio between ρ, the foam apparent density (kg/m^3), and ρ_S, the density of the cells' material (set equal to 1200 kg/m^3). Moreover, *C* and *C*′ are two proportionality constants, fitted by experimental data, and φ is the solid volume fraction contained in the cell edges. The purpose of using such a model was to improve the comprehension of how the filler influenced the structure, and thus the factor φ. In detail, using two different constraints, $\varphi = 1$ (the material is all condensed on the edges – open foam) and $\varphi = 0$ (edges and walls have the same thickness – closed foam), *C* and *C*′ were obtained. Then, for $\varphi = 1$, Eq. (2) becomes (Eq. (3)):

$$\frac{E}{E_S}=C\left(\frac{\rho}{\rho_S}\right)^2 \quad (3)$$

Applying Eq. (3), *C* can be determined for each sample. However, also the exponent of the relative density plays a key role in determining whether the foam is more open- or closed-cells. A more general equation can be obtained considering $C = 1$, usually used in the standard Gibson-Ashby model (Eq. (4)) [38]:

$$\frac{E}{E_S}=C\left(\frac{\rho}{\rho_S}\right)^n \quad (4)$$

where the exponent *n* is determined depending on the foam considered.

Then, from Eq. (2) and Eq. (4) and considering $\varphi = 0$, also *C*′ can be obtained for each foam. A more general equation can be written as Eq. (5):

$$\frac{E}{E_S}=C\varphi^2\left(\frac{\rho}{\rho_S}\right)^n+C'(1-\varphi)\left(\frac{\rho}{\rho_S}\right) \quad (5)$$

from where the φ value of each foam was evaluated, providing a more complete description of the foam structures. Acquired data from mechanical compression tests (namely Young modulus, E, and density, ρ) were, then, used for data processing by means of OriginPro® 2018

(Origin Lab Coorporation, MA, USA).

4. Results and discussion

4.1. Characterization of polyol-grafted CNC (*m*_Ci)

Bio-based polyols with different OH numbers (OH_n ranging from 78 to 297 mg KOH/g), different molar masses (M_w ranging from 870 to 5200 g/mol, see the details of polyols' characterization in S2, SM), and coming from different renewable sources (cardanol, sunflower, linseed and mustard oil) were used to functionalize CNC in homogenous environment through solubilization in DMAc/LiCl system (solution at 2 wt %) [39–41]. The solubilization of CNC in DMAc/LiCl system led to the formation of strong hydrogen bonds between the hydroxyl protons of CNC and the Cl^- anions, allowing the breaking of the hydrogen bond network in CNC along with the splitting of Li^+ Cl^- ions pairs and consequently CNC solubilization [42]. The crystalline domains of CNC (rigid network in which hydrogen interactions exist) are disaggregated and replaced by a silane-cellulose network during homogeneous environmental functionalization. The residual available silane active groups (after CNC functionalization) acted as coupling agents between CNC and polyol (Scheme 1).

4.1.1. Spectroscopic characterization

As an example, the XRD curves of CNC after functionalization (*m*_C1) and that of vacuum-dried pristine CNC are compared in Fig. 1.

Vacuum-dried pristine CNC showed diffraction peaks at 2θ = 16.2°, 22.5° and 34.6° at (110), (200) and (0 0 4) planes, respectively, corresponding to the characteristic peaks of cellulose-I structure [43], where strong H-bonds (intra- and inter-chain) and weaker inter-sheet interactions, such as CH···O H-bonding and van der Waals forces, prevailed [44]. In *m*_C1 (Fig. 1, red curve) a shift of the two peaks from 22.5° to 21° and from 16.2° to 8° was observed. In addition, where a reduction of H-bonds interaction occurred, the diffraction peaks appeared broader and with decreased intensity, demonstrating a noticeable disappearance of its crystalline structure.

All *m*_Ci were analysed by FT-IR (Fig. 2). The strong modification of the IR spectrum of *u*_C gives a clear indication that the functionalization occurred.

The typical stretching vibration broad band of the O—H functional group (3500–3200 cm^{-1}) along with the CH_2 scissoring motion (1430 cm^{-1}) and stretching vibrations of C—O, C–O–C of glycosidic moiety and out of plane stretching vibration (1150–1030 cm^{-1}) were detected for the *u*_C [26,35,45–48]. The spectra of modified CNC samples highlight, in addition to the aforementioned vibration bands, a strong increase of signals between 2900 and 2800 cm^{-1} due to C—H stretching vibration of polyols together with the appearance of two further peaks: one at 1742 cm^{-1} and a second one at 1458 cm^{-1} referred to the C═O stretching vibration of carbonyl group belonging to the ester moiety of the polyol and C═C stretching vibration, respectively [35,47,48] (Fig. 2c). The presence of these new bonds proves the occurrence of the functionalization.

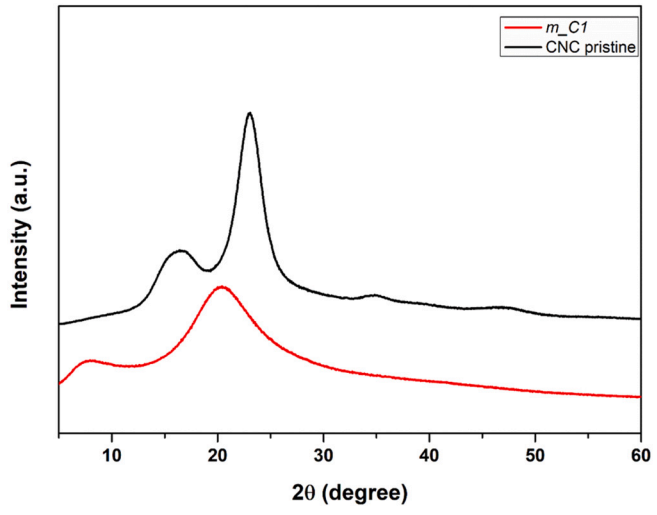

Fig. 1. XRD curves of vacuum-dried CNC (black line) and the selected modified CNC (*m*_C1, red line).

4.1.2. Thermal characterization

TGA and DTGA curves of *m*_Ci are shown in Fig. 3a and b, respectively. *u*_C showed the typical degradation profile of the nanocrystalline cellulose, where the midpoint degradation temperature is around 300 °C (Fig. 3a) [46]. The main degradation process occurs between 260 °C and 310 °C leading to about 70 % of the mass loss (Fig. 3b). Subsequently, a further mass loss around 10 % occurred in the range of 310–400 °C, ascribing to the decomposition of sulphate groups generated during CNC extraction process [46,49]. On the other hand, thermal behaviour of *m*_Ci exhibited an increased midpoint decomposition temperature compared to *u*_C, occurring at 440 °C, approximately (Fig. 3b and Table S2, SM). For *m*_C2 and *m*_C3, a gradual weight loss in the range of 200 °C – 500 °C could be noticed. On the contrary, *m*_C1 presented the highest thermal stability. Overall, the grafting of the bio-based polyols seems to act positively on cellulose thermal stability [50,51].

The average value of mmol of polyol grafted onto *m*_Ci was calculated according to eq. 1. In Table 3, the results are presented as an average and standard deviation of three independent measurements for each sample.

The highest amount of polyol grafted onto CNC was calculated in the sample *m*_C3 by using a polyol with an OH_n of 229 mg KOH/g and a M_w of 870 g/mol, while the lowest one in the case of *m*_C2 (polyol characteristics: OH_n = 297 mg KOH/g, M_w = 5200 g/mol). It seems that the high functionality of polyols makes more sites available for the grafting reaction while the molar mass of polyols appears to influence their diffusion through the reaction medium and within the silane-cellulose network. According to the Stokes-Einstein equation, the diffusion coefficient of a molecule is predicted to increase in inverse proportion to its approximate radius [52]. Therefore, a larger molar mass correlates with a larger approximate radius, so the diffusion coefficient is generally smaller.

For *m*_C2, the "*positive effect*" of the high value of OH_n of polyol RV31 (297 mg KOH/g) comparable to those of *m*_C3 is mitigated by the effect generated by the high molar mass (M_w = 5200 g/mol). Indeed, "*the adverse molar mass effect*" seems to penalize the quantity of grafted polyol and could be attributed to the elevated steric hindrance which limits the access of polyol to the silane-cellulose network [53]. This consideration could be extended to *m*_C1 where the lower molar mass of polyol RV33 compared to RV31 gave a higher amount of polyol grafted to cellulose despite its very low OH_n value. The cellulosic content in 100 g of product after modification, approximately estimated through TGA analysis, was found between 40 and 60 wt% (see Table S2 in SM, paragraph S4).

4.1.3. Morphological characterization

SEM images of CNC after freeze-drying (*u*_C) and after modification (*m*_Ci) are presented in Fig. 4. Vacuum-dried pristine CNC presented a rod-shape-like morphology as reported elsewhere [54,55], although after freeze-drying (*u*_C) assumed a lamellar-like structure [56] suggesting possible agglomeration due to strong hydrogen bonds upon freeze-drying [57]. It could be noticed that the silanization and the subsequent polyol grafting led to important morphological variations of the obtained modified CNCs. Specifically, depending on the grafted bio-based polyols, *m*_Ci assumed various morphological patterns from dense clumping to packed systems.

Dispersion of *m*_C3 within *Component A* (polyols and additives) was qualitatively investigated through optical images to evaluate CNC

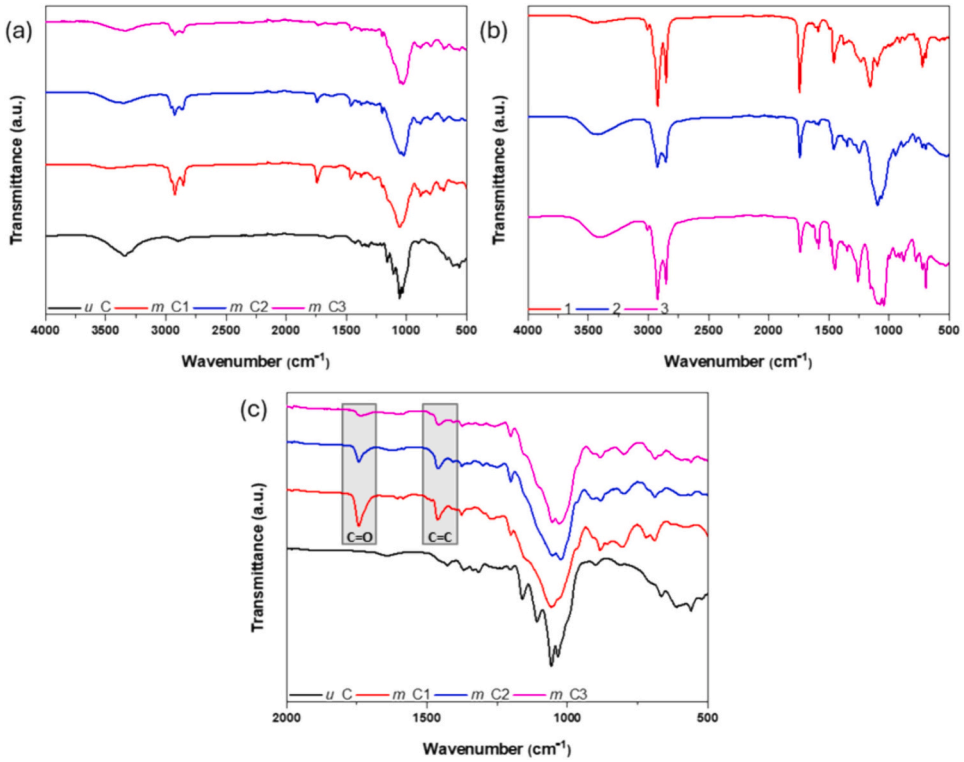

Fig. 2. (a) Overlapped FT-IR spectra of *m*_Ci and *u*_C, (b) overlapped FT-IR spectra of polyols and (c) overlapped FT-IR spectra of *m*_Ci and *u*_C in spectral range 2000–500 cm^{-1}.

dispersion in the polyurethane formulations upon functionalization. Results demonstrate that *m*_C3 formed smaller aggregates compared to *u*_C, implying that the polyol grafting discouraged solid/solid interactions within *u*_C particles, favoured by strong hydrogen bonds. On the other hand, *m*_Ci presented higher dispersibility in *Component A*, which is a non-polar-based solution, corresponding to reduced hydrogen bonds and enhanced liquid/solid interactions [58] (Fig. 5).

*m*_Ci were then added in the bio-based polyurethane foam formulations at three different concentrations: 1, 2, and 3 wt%.

4.2. Characterization of bio-based composite PU foams

4.2.1. Spectroscopic characterization

FT-IR spectra of foams reinforced with 1 wt% of modified and unmodified CNCs are shown in Fig. 6a and compared to that of PU-Pristine. Spectra highlighted no significant differences among the reference PU foams reinforced with *u*_C and those with the *m*_Ci. Two main regions were identified: the first one in the range of 3500–2250 cm^{-1} and the second one between 1700 and 800 cm^{-1}. Characteristic peaks of O—H and C—H stretching vibration were identified at about 3400 cm^{-1} (broad absorption band) and 2700 cm^{-1}, respectively. In the region between 1700 cm^{-1} and 800 cm^{-1} the typical peaks correlated to the urethane groups, the carbonyl (C=O) vibration between 1700 and 1600 cm^{-1}), C-O-C vibration around 1200–100 cm^{-1} and carbamate (C—N) vibration at 1611 cm^{-1} were recognized. The presence of peaks correlated to urethane linkages, as well as the absence of the signal at 2300 cm^{-1} of free NCO groups, indicates complete polymerization. No differences in FT-IR spectra of the selected composite foams (PU_*m*_C3_y) were noticed by increasing CNC concentration (Fig. 6b).

4.2.2. Thermal characterization

Thermal degradation behaviour of the selected PU foams typically presented three degradation stages i.e., a first stage, occurring in the range of 150–300 °C, associated with water evaporation and low molar mass components degradation, a second stage, occurring in 350–450 °C, corresponds to the degradation of urethane bonds, which generate polyol segments, isocyanate and secondary complex products [16]. Further degradation stage was observed in the range > 450 °C, where degradation of higher molar mass components occurred [59,60]. In Table 4, $Tmax_1$, $Tmax_2$, and $Tmax_3$ i.e. the maxima of the derivative function in the range of 150–300 °C, 300–450 °C and 450–500 °C, respectively, and the residual mass at 800 °C, are displayed.

The addition of *u*_C and *m*_Ci had no significant influence on the degradation mechanism. Moreover, CNC functionalization seemed to not significantly modify the thermal stability of the bio-based PU foams with respect to the foams reinforced with *u*_C. However, an important effect could be noticed with respect to PU-pristine, while the highest thermal stability was attained for the case of PU_*m*_C3 with an increase of $Tmax_1$ of 9.5 %, $Tmax_2$ of 3.6 % and $Tmax_3$ of 8.7 %, respectively. These findings were also in agreement with those reported by Onbattuvelli et al. [61] and Coccia et al. [26]. This improved thermal stability is likely the result of cross-linked segments induced by interactions between the polyol OH groups onto the CNC surface and the foam matrix [62,63].

The effect of concentration on the PU foam thermal stability is shown in Table S3 of Section S5 in SM, for the case of *m*_C3. Under the investigated conditions, the concentration of *m*_Ci seemed to not affect the thermal stability of the resulting composite foams.

4.2.3. Morphological characterization

The morphological characteristics of the composite PU foams at 1 wt % of *m*_Ci are displayed in Fig. 7 and compared with those of unloaded and unmodified CNC-composite foams (Fig. 7a and b). Size distribution is shown as an inset. Higher magnification images are also shown to examine *m_Ci* dispersion within cell struts. The average size and number of cells per unit of surface are reported in Table 5.

Small agglomerates are largely visible in PU *u*_C foam (magnification in Fig. 7b). The number of the agglomerates was found to be lower for all

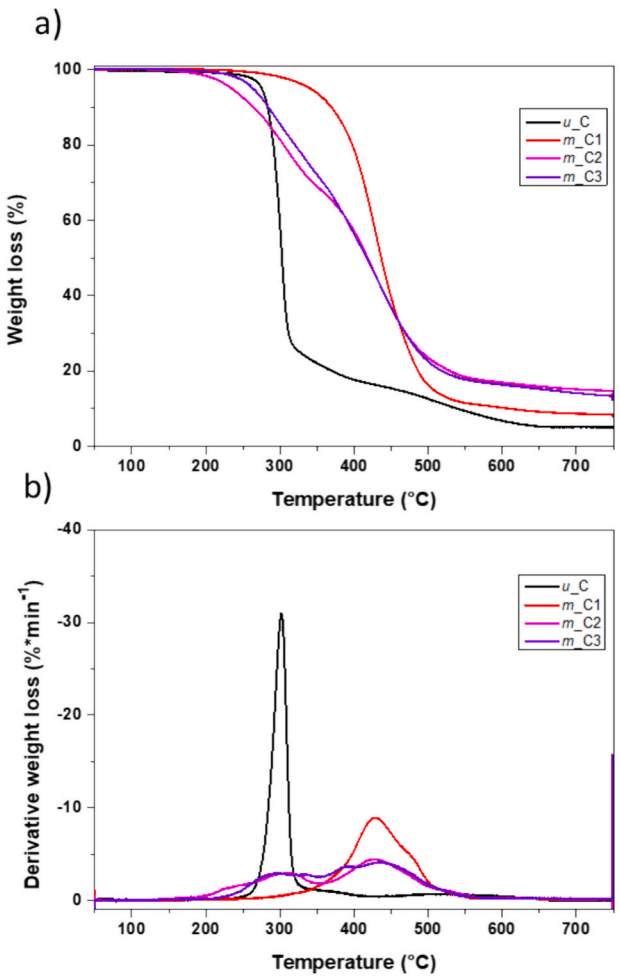

Fig. 3. a) TGA and b) DTGA analysis of unmodified (*u*_C) and modified CNC (*m*_Ci).

Table 3
Results of the mmol/g of polyol after CNC functionalization.

Sample	Grafted polyol (mmol /g_{sample})
*m*_C1	0.170 ± 0.020
*m*_C2	0.050 ± 0.005
*m*_C3	0.320 ± 0.041

the *m*_Ci than *u*_C foams, suggesting an improved dispersibility, as already stated. This implies that *m*_Ci were strongly compatibilized with PU systems turning out to be a reactive reagent within PU formulations and leading to homogeneous foamed systems.

For all tested foams, semi-rigid structures were obtained as both open and closed cells could be identified [16,26,64]. CNC dispersion seems to affect the morphology of PU composite foams leading to a decrease in cell size and distribution with respect to the unloaded foam (Table 5 and Fig. 7a). More specifically, the addition of *u*_C corresponds to an average cell size of 331 ± 140 μm and number of cells per unit of surface equal to 1.3 ± 0.2 10^{-4} μm^{-2} (Table 5, Fig. 7b). Significant differences must be noted according to the different bio-based polyol used in the functionalization route. The dispersion of *m*_C1 and *m*_C2 in the PU foam matrix induced comparable results with respect to the *u*_C, due to the low amount of grafted polyol and thus poor dispersion with the polyol mixture (Table 5). Instead, a decrease in cell size accompanied by a reduction in cell size distribution was noted, in PU_*m*_C3_1 (261 ± 92 μm), along with a remarkable increase of the number of cells per unit of surface (almost 10 fold) with respect to the unloaded and the other composite foams (Table 5). The lowest cell size distribution and the highest cell number per unit of surface was achieved by dispersing *m*_C3, corresponding to the cellulosic system with the highest polyol amount. This behaviour was certainly ascribed to an improved interaction between CNC and PU matrix and to the nucleating effect of *m*_C3, corresponding to a decrease in bubble coalescence [26,65] and thus leading to the formation of more nucleating sites and higher cell numbers [17,66] (Fig. 7e). Since the morphology depends on the concentration and molar mass of both soft and hard segments in PU foam [66], the incorporation of *m*_Ci, containing polyols with different molar masses and functionality, influences the crosslinking density of PU materials resulting in variation of cellular characteristics [67]. Results can be qualitatively compared with previous works concerning the dispersion of CNC in rigid or semi-rigid PU foams, whereas, the functionalization and/or dispersion routes allowed the so-modified CNC to act as a nucleating agent, resulting in finer cellular structure and consequently in advanced functional properties [68].

4.2.4. Mechanical characterization

Compressive tests were performed on at least four different specimens for each sample. Stress-strain curves of composite foams loaded with 1 wt% of *m*_Ci are reported in Fig. 8a. Results of the calculation based on the modified Gibson-Ashby model are shown in Fig. 8b. The morphological, physical, and mechanical properties of PU_*m*_C_1 are displayed in Table 5. Results of composite foams loaded with 2 wt% and 3 wt% are reported in Table S4 in SM.

All the analysed materials exhibited the typical behaviour of elastomeric foams. The properties of the composite foams depend on both the concentration and the chemistry of *m*_Ci, resulting in different values of compressive strength (evaluated at 10 % deformation, $\sigma_{10\%}$) and elastic modulus (Table 4).

In particular, when *u*_C, *m*_C1, and *m*_C2 were added to PU formulation, an increase in mechanical properties was observed at higher concentrations (Table 5 and Table S4, SM).

The best result was observed for foams reinforced with *m*_C3 (corresponding to the highest amount of grafted polyol). For these samples containing *m*_C3, E_{mod} and $\sigma_{10\%}$ resulted the highest registered among the composites, being more than five times higher than those of the unmodified one, especially with concentration of 1 and 2 wt% (Table 5 and Table S4, SM). The evaluation of the specific elastic modulus (E/ρ), and strength (σ/ρ), respectively obtained by dividing E_{mod} and $\sigma_{10\%}$ with the density of the relative foam, highlights an astonishing improvement of mechanical properties with respect to the PU-pristine. It could be detected even for the lowest amount of CNC content. This behaviour could be attributed to the dimension shifting experienced by cell size, which exhibited a strong dimensional reduction as observed from SEM analysis (Fig. 7) [41,69].

Differently from the compressive response observed by Stanzione et al., where PU foams reinforced with amorphous cellulose presented lower $\sigma_{10\%}$ and compressive elastic modulus (E_{mod}, MPa) values compared to the pristine PU foam, in this study, PU-pristine presented the lowest E_{mod} and $\sigma_{10\%}$ among all composite foams (Table 5). Therefore, although functionalization caused a partial amorphization of CNC, it is noteworthy to point out a remarkable reinforcing effect of the examined systems. It should be highlighted that, the addition of 1 wt% *m*_C3 led to more significant improvement of the compressive properties of composite foams compared with the case of modified CNCs through heterogeneous conditions, whereas, a remarkable effect was noted only at 3 wt% of the modified CNCs [26]. This can be ascribed to either good interaction between modified CNC surface and polyurethane matrix, probably due to the larger polyol's amount bonded to cellulose which acted as compatibilizer and/or to the presence of strong silane-cellulose network that replaces the crystalline domines of CNC upon functionalization.

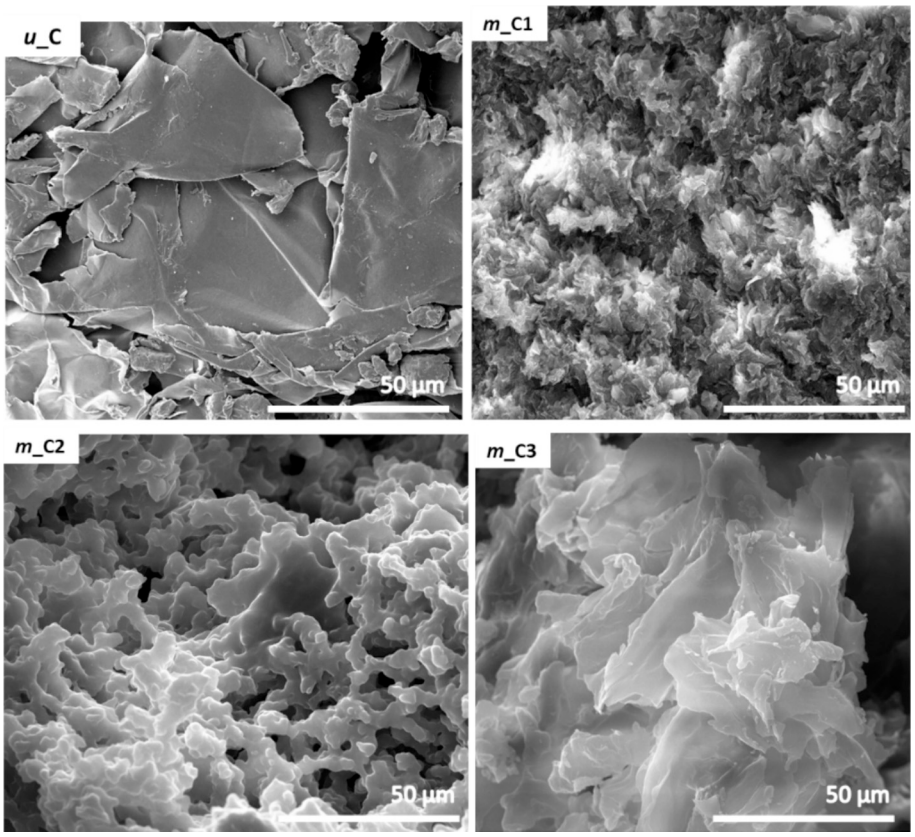

Fig. 4. SEM images of the modified CNCs (*m*_Ci) and of the unmodified CNCs (*u*_C). Magnification 2500×, scale bar = 50 µm, acceleration voltage = 20 kV.

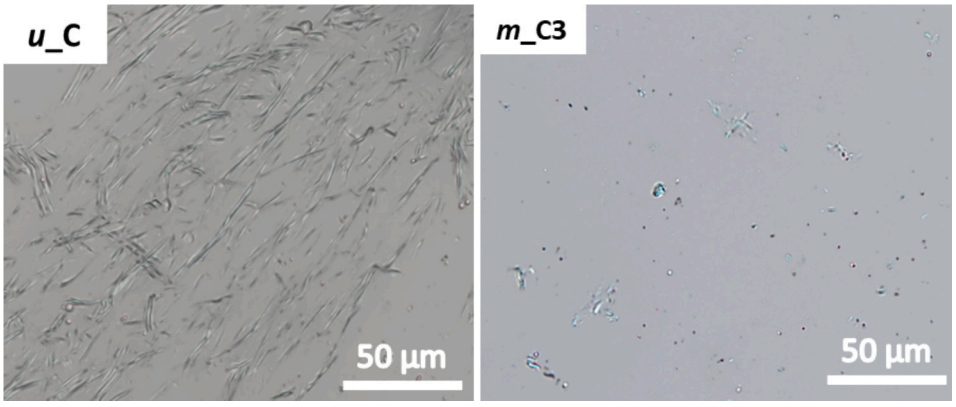

Fig. 5. Optical images of *u*_C, and *m*_C3 dispersed in Component A before foaming process. Magnification:20 X, scale bar = 50 µm.

4.3. Modelling

For a more in-depth evaluation, a modified version of the Gibson-Ashby model was considered. In particular, Eq. (5) was solved for φ as a variable, by using the values reported in Table 6 and Table S4 in SM. The graphical representations of the models are depicted in Figs. 8b, S3c and S4c in SM.

This model provides a clearer picture of the stiffening effect attributed to the effect of *u*_C or *m*_Ci on the cell edges and walls of the resulting composite foams [26].

Different φ resulted from the model, depending on the examined foams (Table 6). Being the value of φ correlated to the distribution of the contribution of edges and walls to the foam stiffness, it was possible to observe a wide spectrum of values. The highest value was attributed to the PU_*u*_C_1, whereas the edges had the strongest impact on the stiffness of the material. On the contrary, all the composite foams exhibited a lower value, meaning that, the presence of *m*_Ci allowed the walls to take part in the mechanical behaviour of the material. Among them, the lowest values of φ were found by using *m*_C3, corresponding to the highest compatibility of the modified CNC with the PU matrix and hence to improved stress distribution among CNC and PU matrix.

5. Conclusions

In this work, CNC functionalization through silanization and subsequent polyol grafting in homogeneous environment was studied aiming to enhance the compatibility and interfacial adhesion between the hydrophobic PU and hydrophilic CNC. It was found that the homogeneous environment provided an adequate number of available OH groups of CNC, resulting in an amount of grafted polyol five times higher than that

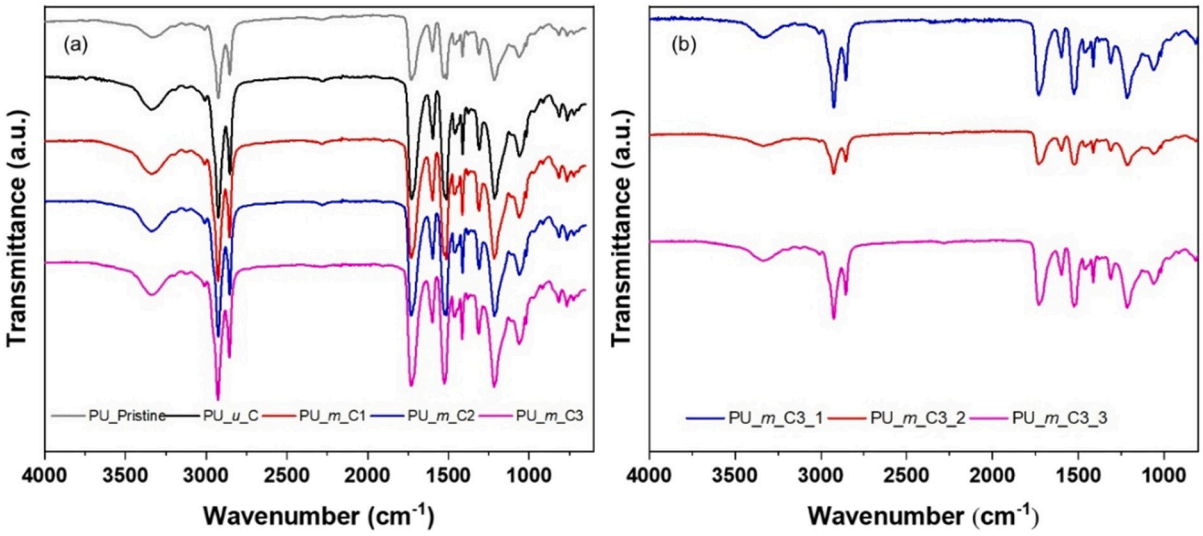

Fig. 6. a) FT-IR spectra for selected polyurethane foams reinforced with *m*_Ci and *u*_C at 1 wt%. The spectrum of PU unloaded foam is presented. b) FT-IR spectra of composite PU foams at different concentrations (1, 2 and 3 wt%) of the selected CNC (*m*_C3).

Table 4
Thermal properties of PU foams reinforced with 1 wt% modified CNCs (PU_*m*_*Ci*_1).

Sample	$Tmax_1$ (°C)	$Tmax_2$ (°C)	$Tmax_3$ (°C)	Char at 800 °C (wt%)
PU-pristine	280.2	345.8	426.7	Negligible
PU_*u*_C_1	304.2	355.2	458.3	7.0
PU_*m*_C1_1	305.4	351.5	421.2	7.3
PU_*m*_C2_1	309.2	355.9	460.8	6.5
PU_*m*_C3_1	309.8	357.9	465.7	8.1

obtained in a heterogeneous environment. In homogeneous environment, the crystalline domains of CNC (rigid network in which hydrogen interactions exist) are disaggregated and replaced by a silane-cellulose network which is formed due to the interaction between the reactive groups of the silane (chlorides) and the OH groups of CNC. Finally, the residual available silane active groups (after cellulose functionalization) acted as a coupling agent between CNC and polyol. A crucial factor affecting polyol grafting is its diffusion capacity in the silane-cellulose network, which is influenced by both the M_w and the OH number of the polyols in opposite ways. For comparable OH numbers, a higher M_w invalidates the polyol diffusion making the grafting on silane-cellulose sites difficult.

As a result of the solubilization and silane-polyol grafting, a partial amorphization of CNC occurred, transforming CNC into a reactive reagent able to react with PU precursors thanks to the polyol moiety grafted to CNC. The enhancement of CNC dispersion in the PU matrix due to an increased interaction filler-matrix led to an improvement of

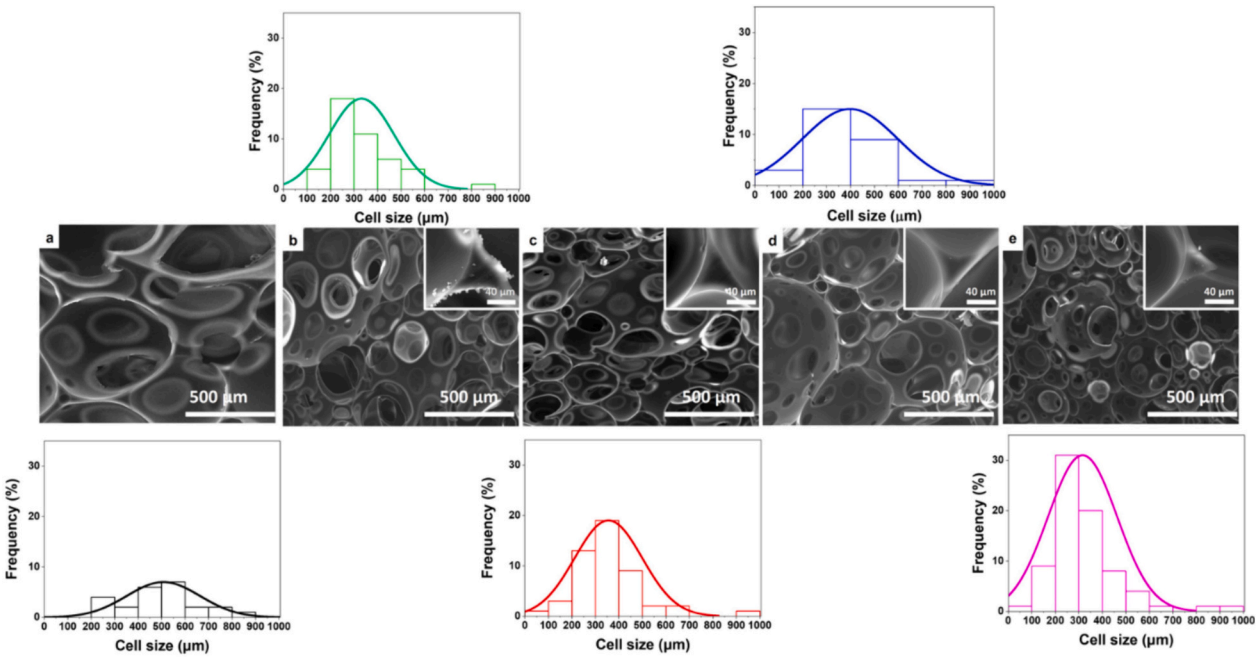

Fig. 7. a-e) SEM images of unloaded (a) and the selected composite PU foams at 1 wt% (PU_*m*_Ci_1). b) PU_*u*_C_1, c) PU_*m*_C1_1, d) PU_*m*_C2_1, e) PU_*m*_C3_1. Magnification 200 X. Scale bar = 500 μm. Insets: higher magnification images (magnification 3000 X, scale bar = 40 μm, acceleration voltage = 20 kV). As insets: cell size distribution of the selected composite PU foams, evaluated via Image J software. For each sample 100 different cells were taken into consideration.

Table 5
Physical, morphological, and structural properties of 1 wt% of bio-based unloaded and composite PU foams.

Samples	Apparent density, ρ, (kg/m^3)	Average size (μm)	Number of cells (1/ μm^2•10^{-4})	σ 10%Ⅱ, (kPa)	Emod Ⅱ, (MPa)	σ/ρ, (kPa/(kg/m^3)	E/ρ, (kPa/(kg/m^3)
PU-pristine	107.9 ± 1.8	507 ± 150	0.5 ± 0.1	48.8 ± 0.2	0.71 ± 0.04	0.45	6.58
PU_*u*_C_1	101.3 ± 0.3	331 ± 140	1.3 ± 0.2	59.1 ± 9.0	0.88 ± 0.25	0.58	8.72
PU_*m*_C1_1	114.1 ± 1.4	355 ± 144	1.2 ± 0.1	57.4 ± 1.4	0.95 ± 0.10	0.50	8.32
PU_*m*_C2_1	109.3 ± 1.5	398 ± 180	1.6 ± 0.3	57.4 ± 2.3	1.05 ± 0.08	0.53	9.60
PU_*m*_C3_1	175.1 ± 1.6	261 ± 92	9.6 ± 0.8	255.9 ± 4.2	4.81 ± 0.85	1.46	27.46

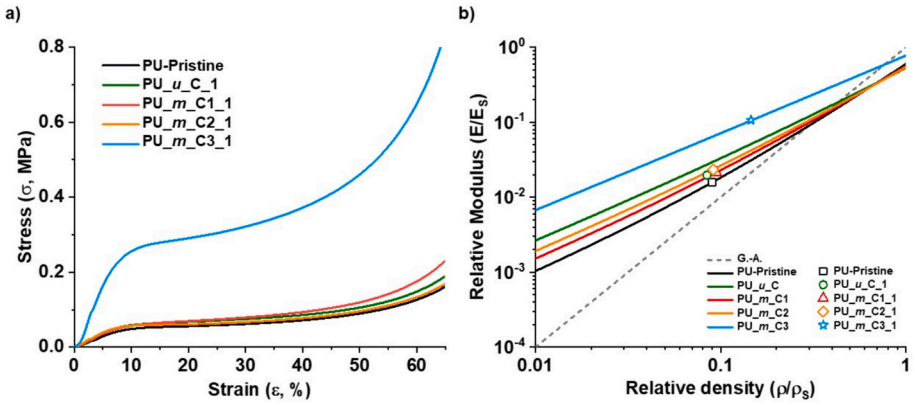

Fig. 8. a) Stress-strain curves of PU_*m*_Ci_1. As references, PU-unloaded (PU-Pristine, black) and PU_*u*_C_1 (green), are reported, b) a graphical representation of the modified Gibson-Ashby model for the selected composite foams.

Table 6
Outcomes of the Gibson-Ashby model of the selected PU foams.

Samples	ρ/ρS (−)	E/ES (−)	n	C	C′	φ
PU-pristine	0.090	0.016	1.723	1.950	0.175	0.513
PU_*u*_C_1	0.084	0.020	1.590	2.754	0.232	0.363
PU_*m*_C1_1	0.095	0.021	1.640	2.333	0.222	0.429
PU_*m*_C2_1	0.091	0.023	1.569	2.810	0.256	0.356
PU_*m*_C3_1	0.146	0.107	1.162	5.017	0.732	0.199

mechanical properties of composite foams. The best results were achieved for *m*_C3, whereas E_{mod} and $\sigma_{10\%}$ were found to be more than five times higher than PU_unloaded and PU_*u*_C, especially at increased cellulose concentration (2 wt%). A modified version of the Gibson-Ashby model was considered to correlate the foam morphological characteristics with their mechanical properties. The estimated φ-parameter was a measure of the stress distribution between the modified CNC and the polymer matrix. The lowest value of φ was found for the case of PUs reinforced with *m*_C3, where the highestcompatibility of the modified systems with the PU matrix was reached, resulting in well-distributed stress between modified CNC and PU matrices. In conclusion, this manuscript explores a new approach to functionalized CNC that, although it appears amorphous at the end of the functionalization step, can be used as a reinforcing agent in polyurethane foams.

Moreover, the enhancement of mechanical properties of the resulting composite foams through the incorporation of such modified CNC could further broaden the use of these materials in construction or packaging sectors.

Financial support

This research was supported by EU Horizon 2020 research and Innovation Program BIOMAT project, GA number: No 953270.

CRediT authorship contribution statement

Selena Silvano: Writing – review & editing, Writing – original draft, Validation, Methodology, Investigation. **Pierluigi Moimare:** Validation, Methodology, Investigation. **Liudmyla Gryshchuk:** Validation, Methodology, Investigation. **Einav Barak-Kulbak:** Resources. **Federica Recupido:** Writing – review & editing, Writing – original draft, Methodology, Investigation. **Giuseppe Cesare Lama:** Writing – review & editing, Writing – original draft, Software, Investigation. **Laura Boggioni:** Writing – review & editing, Writing – original draft, Validation, Supervision, Project administration, Methodology, Investigation, Funding acquisition. **Letizia Verdolotti:** Writing – review & editing, Writing – original draft, Validation, Supervision, Project administration, Methodology, Investigation, Funding acquisition.

Declaration of competing interest

The authors declare that they have no known competing financial interests or personal relationships that could have appeared to influence the work reported in this paper.

Acknowledgments

The authors acknowledge AEP Polymers S.R.L. for the free supply of polyols.

Appendix A. Supplementary data

Supplementary data to this article can be found online at https://doi.org/10.1016/j.ijbiomac.2024.135282.

References

[1] L. Thompson, J. Azadmanjiri, M. Nikzad, S. Igor, J. Wang, A. Yu, Cellulose nanocrystals: production, functionalization and advanced applications, RAMS 58 (1) (2019) 1–16, https://doi.org/10.1515/rams-2019-0001.
[2] Grand View Research, Polyurethane Market Size, Share & Trends Analysis Report By Product (Rigid Foam, Flexible Foam), By End-use (Electronics & Appliances,

Packaging), By Region, And Segment Forecasts, 2023–2030, 2023 https://www.grandviewresearch.com/industry-analysis/polyurethane-pu-market. (accessed 10 april 2023).
[3] W. Leng, J. Li, Z. Cai, Synthesis and characterization of cellulose Nanofibril-reinforced polyurethane foam, Polymers 9 (11) (2017) 597, https://doi.org/10.3390/polym9110597.
[4] F. de Luca Bossa, L. Verdolotti, V. Russo, P. Campaner, A. Minigher, G.C. Lama, L. Boggioni, R. Tesser, M. Lavorgna, Upgrading sustainable polyurethane foam based on greener polyols: succinic-based polyol and Mannich-based polyol, Materials 13 (14) (2020) 3170, https://doi.org/10.3390/ma13143170.
[5] L. Verdolotti, S. Colini, G. Porta, S. Iannace, Effects of the addition of LiCl, LiClO4, and LiCF3SO3 salts on the chemical structure, density, electrical, and mechanical properties of rigid polyurethane foam composite, Polym. Eng. Sci. 51 (6) (2011) 1137–1144, https://doi.org/10.1002/pen.21846.
[6] L. Verdolotti, E. Di Maio, M. Lavorgna, S. Iannace, L. Nicolais, Polyurethane–cement-based foams: Characterization and potential uses, J Appl Polym Sci 107 (2008) 1–8, https://biblioproxy.cnr.it:2481/10.1002/app.24997.
[7] T. Zhai, L. Verdolotti, S. Kacilius, P. Cerruti, G. Gentile, H. Xia, M. Stanzione, G. G. Buonocore, M. Lavorgna, High piezo-resistive performances of anisotropic composites realized by embedding rGO-based chitosan aerogels into open cell polyurethane foams, Nanoscale 11 (18) (2019) 8835–8844, https://doi.org/10.1039/C9NR00157C.
[8] J. Peyrton, C. Chambaretaud, A. Sarbu, L. Avérous, Biobased polyurethane foams based on new polyol architectures from microalgae oil, ACS Sustain. Chem. Eng. 8 (32) (2020) 12187–12196, https://doi.org/10.1021/acssuschemeng.0c03758.
[9] L. Verdolotti, M.R. Di Caprio, M. Lavorgna, G. G. Buonocore, Ch.9 - Polyurethane nanocomposite foams: correlation between nanofillers, porous morphology, and structural and functional properties, Ed: S., et al Polyurethane Polymers, Elsevier, 277–310 (2017). ISBN 9780128040652. doi:1016/B978-0-12-804065-2.00009-7.
[10] O. Daglar, U.S. Gunay, G. Hizal, U. Tunca, H. Durmaz, Extremely rapid Polythioether synthesis in the presence of TBD, Macromolecules 52 (9) (2019) 3558–3572, https://doi.org/10.1021/acs.macromol.9b00293.
[11] J. Peyrton, L. Avérous, Structure-properties relationships of cellular materials from biobased polyurethane foams, Mater. Sci. Eng. R. Rep. 145 (2021) 100608, https://doi.org/10.1016/j.mser.2021.100608.
[12] N.S. Purwanto, Y. Chen, J.M. Torkelson, Reprocessable, bio-based, self-blowing non-isocyanate polyurethane network foams from cashew nutshell liquid, ACS Appl. Polym. Mater. 5 (8) (2023) 6651–6661, https://doi.org/10.1021/acsapm.3c01196.
[13] F. de Luca Bossa, C. Santillo, L. Verdolotti, P. Campaner, A. Minigher, L. Boggioni, S. Losio, F. Coccia, S. Iannace, G.C. Lama, Greener nanocomposite polyurethane foam based on sustainable polyol and natural fillers: investigation of Chemico-physical and mechanical properties, Materials 13 (1) (2020) 211, https://doi.org/10.3390/ma13010211.
[14] F. Recupido, G.C. Lama, M. Ammendola, F.D.L. Bossa, A. Minigher, P. Campaner, A.G. Morena, T. Tzanov, M. Ornelas, A. Barros, F. Gomes, V. Bouça, R. Malgueiro, M. Sanchez, E. Martinez, L. Sorrentino, L. Boggioni, M. Perucca, S. Anegalla, R. Marzella, P. Moimare, L. Verdolotti, Rigid composite bio-based polyurethane foams: from synthesis to LCA analysis, Polymer 267 (2023) 125674, https://doi.org/10.1016/j.polymer.2023.125674.
[15] A. Pascarella, F. Recupido, G.C. Lama, L. Sorrentino, A. Campanile, B. Liguori, M. Berthet, G. Rollo, M. Lavorgna, L. Verdolotti, Design and development of sustainable polyurethane foam: a proof-of-concept as customizable packaging for cultural heritage applications, Adv. Eng. Mat. 26 (7) (2024) 2301888, https://doi.org/10.1002/adem.202301888.
[16] X. Zhou, M.M. Sain, K. Oksman, Semi-rigid biopolyurethane foams based on palm-oil polyol and reinforced with cellulose nanocrystals, Compos. - A: App. Sci. Manuf. 83 (2016) 56–62, https://doi.org/10.1016/j.compositesa.2015.06.008.
[17] J. Liang, T. Zhou, Y. Fu, G. Tian, Y. Zhang, Z. Wang, Pretreated cellulose fiber for enhancing fire resistance of flexible polyurethane foam composites with reinforced properties, Ind. Crop. Prod. 205 (2023) 117429, https://doi.org/10.1016/j.indcrop.2023.117429.
[18] M. Ghasemlou, F. Daver, E.P. Ivanova, Y. Habibi, B. Adhikari, Surface modifications of nanocellulose: from synthesis to high-performance nanocomposites, Prog. Polym. Sci. 119 (2021) 101418, https://doi.org/10.1016/j.progpolymsci.2021.101418.
[19] M. Mariano, N. El Kissi, A. Dufresne, Cellulose nanocrystals and related nanocomposites: review of some properties and challenges, J Polym Sci B 52 (12) (2014) 791–806, https://doi.org/10.1002/polb.23490.
[20] M. Stanzione, M. Oliviero, M. Cocca, M.E. Errico, G. Gentile, M. Avella, M. Lavorgna, G.G. Buonocore, L. Verdolotti, Tuning of polyurethane foam mechanical and thermal properties using ball-milled cellulose, Carbohyd. Polym. 231 (2020) 115772, https://doi.org/10.1016/j.carbpol.2019.115772.
[21] A.A. Septevani, D.A.C. Evans, D.J. Martin, P. Song, P.K. Annamalai, Tuning the microstructure of polyurethane foam using nanocellulose for improved thermal insulation properties through an efficient dispersion methodology, Polym. Compos. 44 (12) (2023) 8857–8869, https://doi.org/10.1002/pc.27743.
[22] T. Heinze, T. Liebert, Unconventional methods in cellulose functionalization, Prog. Polym. Sci. 26 (2001) 1689–1762, https://doi.org/10.1016/S0079-6700(01)00022-3.
[23] J. Tang, J. Sisler, N. Grishkewich, K.C. Tam, Functionalization of cellulose nanocrystals for advanced applications, J. Colloid Interface Sci. 494 (2017) 397–409, https://doi.org/10.1016/j.jcis.2017.01.077.
[24] M. Ramesh, L. Rajeshkumar, G. Sasikala, D. Balaji, A. Saravanakumar, V. Bhuvaneswari, R. Bhoopathi, A critical review on wood-based polymer composites: processing, properties, and prospects, Polymers 14 (3) (2022) 589, https://doi.org/10.3390/polym14030589.
[25] T. Nowak, B. Mazela, K. Olejnik, B. Peplińska, W. Perdoch, Starch-silane structure and its influence on the hydrophobic properties of paper, Molecules 27 (10) (2022) 3136, https://doi.org/10.3390/molecules27103136.
[26] F. Coccia, L. Gryshchuk, P. Moimare, F.L. Bossa, C. Santillo, E. Barak-Kulbak, L. Verdolotti, L. Boggioni, G.C. Lama, Chemically functionalized cellulose nanocrystals as reactive filler in bio-based polyurethane foams, Polymers 13 (15) (2021) 2556, https://doi.org/10.3390/polym13152556.
[27] H. Khanjanzadeh, R. Behrooz, N. Bahramifar, W. Gindl-Altmutter, M. Bacher, M. Edler, T. Griesser, Surface chemical functionalization of cellulose nanocrystals by 3-aminopropyltriethoxysilane, Int. J. Biol. Macromol. 106 (2018) 1288–1296, https://doi.org/10.1016/j.ijbiomac.2017.08.136.
[28] S.P. Bangar, M. Harussani, R. Ilyas, A.O. Ashogbon, A. Singh, M. Trif, S.M. Jafari, Surface modifications of cellulose nanocrystals: processes, properties, and applications, Food Hydrocoll. 130 (2022) 107689, https://doi.org/10.1016/j.foodhyd.2022.107689.
[29] Y. Xie, C.A.S. Hill, Z. Xiao, H. Militz, C. Mai, Silane coupling agents used for natural fiber/polymer composites: a review, Compos. - A: App. Sci. Manuf. 41 (7) (2010) 806–819, https://doi.org/10.1016/j.compositesa.2010.03.005.
[30] B. Koohestani, A. Khodadadi-Darban, P. Mokhtari, E. Yilmaz, E. Darezereshki, Comparison of different natural fiber treatments: a literature review, Int. J. Environ. Sci. Technol. 16 (2018) 1–14, https://doi.org/10.1007/s13762-018-1890-9.
[31] R.A. Chowdhury, C.M. Clarkson, S. Shrestha, S.M. El Awad Azrak, M. Mavlan, J. P. Youngblood, High-performance waterborne polyurethane coating based on a blocked isocyanate with cellulose nanocrystals (CNC) as the polyol, ACS App. Polym. Mater. 2 (2) (2020) 385–393, https://doi.org/10.1021/acsapm.9b00849.
[32] N.M. Girouard, S. Xu, G.T. Schueneman, M.L. Shofner, J.C. Meredith, Site-selective modification of cellulose nanocrystals with Isophorone Diisocyanate and formation of polyurethane-CNC composites, ACS Appl. Mater. Interfaces 8 (2) (2016) 1458–1467, https://doi.org/10.1021/acsami.5b10723.
[33] R.A. Ilyas, S.M. Sapuan, M.L. Sanyang, M.R. Ishak, E.S. Zainudin, Nanocrystalline cellulose as reinforcement for polymeric matrix nanocomposites and its potential applications: a review, Curr. Anal. Chem. 14 (3) (2018) 203–225, https://doi.org/10.2174/1573411013666171003155624.
[34] K. Roy, A. Pongwisuthiruchte, S. Chandra Debnath, P. Potiyaraj, Application of cellulose as green filler for the development of sustainable rubber technology, CRGSC 4 (2021) 100140, https://doi.org/10.1016/j.crgsc.2021.100140.
[35] A. Rachini, M. Le Troedec, C. Peyratout, A. Smith, Comparison of the thermal degradation of natural, alkali-treated and silane-treated hemp fibers under air and an inert atmosphere, J. App. Polym. Sci. 112 (1) (2009) 226–234, https://doi.org/10.1002/app.29412.
[36] B. Fathi, M. Harirforoush, M. Foruzanmehr, S. Elkoun, M. Robert, Effect of TEMPO oxidation of flax fibers on the grafting efficiency of silane coupling agents, J. Mater. Sci. 52 (17) (2017) 10624–10636, https://doi.org/10.1007/s10853-017-1224-1.
[37] L.J. Gibson, M.F. Ashby, The mechanics of foams: Basic results, in: C.U. Press (Ed.), Cellular Solids: Structure and Properties, Cambridge, 1997, pp. 175–234, https://doi.org/10.1017/CBO9781139878326.007.
[38] M.F. Ashby, R. Medalist, The mechanical properties of cellular solids, Metall. Mater. Trans. 14 (9) (1983) 1755–1769, https://doi.org/10.1007/BF02645546.
[39] M. Isik, H. Sardon, D. Mecerreyes, Ionic liquids and cellulose: dissolution, chemical modification and preparation of new cellulosic materials, Int. J. Molec. Sci. 15 (7) (2014) 11922–11940, https://doi.org/10.3390/ijms150711922.
[40] A.S. Gross, A.T. Bell, J.W. Chu, Preferential interactions between lithium chloride and glucan chains in N,N-dimethylacetamide drive cellulose dissolution, J. Phys. Chem. B 117 (12) (2013) 3280–3286, https://doi.org/10.1021/jp311770u.
[41] R. Zhang, J. Chen, Y. Zhu, J. Zhang, G. Luo, P. Cao, Q. Shen, L. Zhang, Correlation between the structure and compressive property of PMMA microcellular foams fabricated by supercritical CO2 foaming method, Polymers 12 (2) (2020) 315, https://doi.org/10.3390/polym12020315.
[42] C. Zhang, R. Liu, J. Xiang, H. Kang, Z. Liu, Y. Huang, Dissolution mechanism of cellulose in N,N-dimethylacetamide/lithium chloride: revisiting through molecular interactions, J. Phys. Chem. B 118 (31) (2014) 9507–9514, https://doi.org/10.1021/jp506013c.
[43] V.K. Thakur, M.K. Thakur, Processing and characterization of natural cellulose fibers/thermoset polymer composites, Carbohydr. Polym. 109 (2014) 102–117, https://doi.org/10.1016/j.carbpol.2014.03.039.
[44] J. Guo, W. Du, S. Wang, Y. Yin, Y. Gao, Cellulose nanocrystals: a layered host candidate for fabricating intercalated nanocomposites, Carbohyd. Polym. 157 (2017) 79–85, https://doi.org/10.1016/j.carbpol.2016.09.065.
[45] M. Beaumont, M. Bacher, M. Opietnik, W. Gindl-Altmutter, A. Potthast, T. Rosenau, A general aqueous silanization protocol to introduce vinyl, mercapto or azido functionalities onto cellulose fibers and nanocelluloses, Molecules 23 (6) (2018) 1427, https://doi.org/10.3390/molecules23061427.
[46] C.F. Bellani, E. Pollet, A. Hebraud, F.V. Pereira, G. Schlatter, L. Avérous, R.E. S. Bretas, M.C. Branciforti, Morphological, thermal, and mechanical properties of poly(ε-caprolactone)/poly(ε-caprolactone)-grafted-cellulose nanocrystals mats produced by electrospinning, J. App. Polym. Sci. 133 (21) (2016), https://doi.org/10.1002/app.43445.
[47] Z. Zhang, G. Sèbe, D. Rentsch, T. Zimmermann, P. Tingaut, Ultralightweight and flexible Silylated Nanocellulose sponges for the selective removal of oil from water, Chem. Mater. 26 (8) (2014) 2659–2668, https://doi.org/10.1021/cm5004164.

[48] N. Özmen, N.S. Çetin, P. Tingaut, G. Sèbe, Transesterification reaction between acetylated wood and trialkoxysilane coupling agents, J. App. Polym. Sci. 105 (2007) 570–575, https://doi.org/10.1002/app.26069.
[49] K. Sahlin, L. Forsgren, T. Moberg, D. Bernin, M. Rigdahl, G. Westman, Surface treatment of cellulose nanocrystals (CNC): effects on dispersion rheology, Cellulose 25 (1) (2018) 331–345, https://doi.org/10.1007/s10570-017-1582-5.
[50] K. Dhali, F. Daver, P. Cass, B. Adhikari, Surface modification of the cellulose nanocrystals through vinyl silane grafting, Int. J. Biol. Macromol. 200 (2022) 397–408, https://doi.org/10.1016/j.ijbiomac.2022.01.079.
[51] T.H. Mekonnen, T. Haile, M. Ly, Hydrophobic functionalization of cellulose nanocrystals for enhanced corrosion resistance of polyurethane nanocomposite coatings, App. Surf. Sci. 540 (2021) 148299, https://doi.org/10.1016/j.apsusc.2020.148299.
[52] J.T. Edward, Molecular volumes and the stokes-Einstein equation, J. Chem. Educ. 47 (4) (1970) 261, https://doi.org/10.1021/ed047p261.
[53] P. Tingaut, R. Hauert, T. Zimmermann, Highly efficient and straightforward functionalization of cellulose films with thiol-ene click chemistry, J. Mater. Chem. 21 (40) (2011) 16066–16076, https://doi.org/10.1039/C1JM11620G.
[54] M. Rasheed, M. Jawaid, B. Parveez, A. Zuriyati, A. Khan, Morphological, chemical and thermal analysis of cellulose nanocrystals extracted from bamboo fibre, Int. J. Biol. Macromol. 160 (2020) 183–191, https://doi.org/10.1016/j.ijbiomac.2020.05.170.
[55] N.H. Mohd, N.F.H. Ismail, J.I. Zahari, W.F.B. Wan Fathilah, H. Kargarzadeh, S. Ramli, I. Ahmad, M.A. Yarmo, R. Othaman, Effect of aminosilane modification on nanocrystalline cellulose properties, J. Nanomat. 2016 (2016) 4804271, https://doi.org/10.1155/2016/4804271.
[56] S. Sinquefield, P.N. Ciesielski, K. Li, D.J. Gardner, S. Ozcan, Nanocellulose dewatering and drying: current state and future perspectives, ACS Sustain. Chem. Eng. 8 (26) (2020) 9601–9615, https://doi.org/10.1021/acssuschemeng.0c01797.
[57] N. Lorwanishpaisarn, P. Sae-Oui, S. Amnuaypanich, C. Siriwong, Fabrication of untreated and silane-treated carboxylated cellulose nanocrystals and their reinforcement in natural rubber biocomposites, Sci. Rep. 13 (1) (2023) 2517, https://doi.org/10.1038/s41598-023-29531-x.
[58] B.M. Trinh, T. Mekonnen, Hydrophobic esterification of cellulose nanocrystals for epoxy reinforcement, Polymer 155 (2018) 64–74, https://doi.org/10.1016/j.polymer.2018.08.076.
[59] D.S.W. Pau, C.M. Fleischmann, M.A. Delichatsios, Thermal decomposition of flexible polyurethane foams in air, Fire Saf. J. 111 (2020) 102925, https://doi.org/10.1016/j.firesaf.2019.102925.
[60] T.M. Nguyen-Ha, T.B. Nguyen, T.A. Nguyen, L.H. Pham, D.H. Nguyen, D. M. Nguyen, D. Hoang, E. Oh, J. Suhr, Novel high-performance sustainable polyurethane nanocomposite foams: fire resistance, thermal stability, thermal conductivity, and mechanical properties, Chem. Eng. J. 474 (2023) 145585, https://doi.org/10.1016/j.cej.2023.145585.
[61] V.P. Onbattuvelli, R.K. Enneti, J. Simonsen, K.H. Kate, V.K. Balla, S.V. Atre, Structure and thermal stability of cellulose nanocrystal/polysulfone nanocomposites, Mater. Today Commun. 22 (2020) 100797, https://doi.org/10.1016/j.mtcomm.2019.100797.
[62] X. Huang, C.F. De Hoop, J. Xie, C.-Y. Hse, J. Qi, T. Hu, Characterization of biobased polyurethane foams employing lignin fractionated from microwave liquefied switchgrass, Int. J. Polym. Sci. 2017 (2017) 4207367, https://doi.org/10.1155/2017/4207367.
[63] F. Recupido, G.C. Lama, M. Lavorgna, G.G. Buonocore, R. Marzella, L. Verdolotti, Post-consumer recycling of Tetra Pak®: starting a “new life” as filler in sustainable polyurethane foams, Food Packaging and Shelf. 40 (2023) 101175, https://doi.org/10.1016/j.fpsl.2023.101175.
[64] K. Skleničková, S. Abbrent, M. Halecký, V. Kočí, H. Beneš, Biodegradability and ecotoxicity of polyurethane foams: a review, Crit. Rev. Environ. Sci. Technol. 52 (2) (2022) 157–202, https://doi.org/10.1080/10643389.2020.1818496.
[65] M. Stanzione, V. Russo, M. Oliviero, L. Verdolotti, A. Sorrentino, M. Di Serio, R. Tesser, S. Iannace, M. Lavorgna, Synthesis and characterization of sustainable polyurethane foams based on polyhydroxyls with different terminal groups, Polymer 149 (2018) 134–145, https://doi.org/10.1016/j.polymer.2018.06.077.
[66] M. Szycher, Structure–Property Relations in Polyurethanes, Szycher’s Handbook of Polyurethanes, CRC Press, Boca Raton, FL, USA, 2012.
[67] S. Członka, A. Strąkowska, K. Strzelec, A. Kairytė, A. Kremensas, Bio-based polyurethane composite foams with improved mechanical, thermal, and antibacterial properties, Materials 13 (5) (2020) 1108, https://doi.org/10.3390/ma13051108.
[68] X. Huang, C.F. De Hoop, J. Xie, Q. Wu, D. Boldor, J. Qi, High bio-content polyurethane (PU) foam made from bio-polyol and cellulose nanocrystals (CNCs) via microwave liquefaction, Mater. Des. 138 (2018) 11–20, https://doi.org/10.1016/j.matdes.2017.10.058.
[69] B.Y. Su, C.M. Huang, H. Sheng, W.Y. Jang, The effect of cell-size dispersity on the mechanical properties of closed-cell aluminum foam, Mater Charact 135 (2018) 203–213.